Available online at www.sciencedirect.com
SCIENCE DIRECT®
Physica B 335 (2003) 77–81
PHYSICA B
www.elsevier.com/locate/physb

Measuring lateral magnetic structures in thin films using time-of-flight polarized neutron reflectometry

W.-T. Lee[a,*,1], F. Klose[a,1], H.Q. Yin[b], B.P. Toperverg[c,d]

[a] *Oak Ridge National Laboratory, Oak Ridge, TN 37831, USA*
[b] *University of Alabama, Tuscaloosa, AL 35487, USA*
[c] *Forschungszentrum Jülich, Jülich D-52425, Germany*
[d] *Petersburg Nuclear Physics Institute, Gatchina 188300, Russia*

Abstract

Polarized neutron reflectometry (PNR) has recently been applied to study lateral magnetic structures such as regular micron-sized magnetic arrays on a surface. To date, however, there is a lack of detailed accounts of the features observed in the scattered intensity map in the special case of time-of-flight (TOF) PNR. We present here preliminary measurement results on lithographically produced arrays of micron-sized rectangular permalloy magnetic bars. The measurements demonstrate the potential of the method to provide detailed structural information on a laterally patterned sample, as well as on its magnetic characteristics. The information can be obtained by analyzing the specular reflection along with three off-specular Bragg sheets. Most of the features seen experimentally can be interpreted by using simple heuristic arguments. In addition, we also present results of a study of lateral magnetic domains in an exchange-biased Co/CoO bilayer film to illustrate the capability of TOF PNR in the study of large lateral magnetic domains in the case when almost no off-specular scattering is detected.

PACS: 61.12.Ha; 61.10.Bt; 75.70.Kw; 75.70.Cn

Keywords: Time-of-flight neutron reflectometry; Off-specular scattering; Specular reflection; Distorted-wave Born approximation; Patterned magnetic arrays; Lateral magnetic domains

One of the techniques used to study magnetic surfaces and thin films is polarized neutron reflectometry (PNR) [1–3]. PNR has conventionally been applied for studying systems in which the magnetic structure consists of a stack of laterally uniform magnetic layers. The measurements reveal the depth dependence of the magnetization, in magnitude as well as in direction. Recently, there has been increasing interest in developing the techniques to measure systems with lateral structures such as arrays of magnetic elements on a surface fabricated by lithography.

In a time-of-flight (TOF) PNR experiment, a polarized neutron beam impinges on a surface at a glancing angle. The reflected neutron intensity is measured as a function of neutron wavelength λ

*Corresponding author. Tel.: +1-630-252-5285; fax: +1-630-252-4163.
E-mail address: wtlee@anl.gov (W.-T. Lee).
[1] Current address: Argone National Laboratory, IL 60439, USA.

0921-4526/03/$ - see front matter © 2003 Elsevier Science B.V. All rights reserved.
doi:10.1016/S0921-4526(03)00195-9

and scattering angle $2\theta = \theta_f + \theta_i$, where θ_i and θ_f are the incident and reflected angles, respectively. The scattering plane is perpendicular to the surface and the beam is usually not well collimated in the direction perpendicular to the scattering plane. In general, the scattering cross-section is a function of the incident beam's wave vector $\boldsymbol{k}_i$ and the scattered neutron's wave vector $\boldsymbol{k}_f$ separately. In the Born approximation (BA) where the scattering is weak, the scattered intensity can be written as a function of the wave vector transfer, $\boldsymbol{q} = \boldsymbol{k}_i - \boldsymbol{k}_f = q_z\boldsymbol{z} + q_x\boldsymbol{x}$, where $\boldsymbol{z}$ is a unit vector perpendicular to the sample surface and $\boldsymbol{x}$ is a unit vector on the intersection line between the sample surface and the scattering plane. The lateral projection of $\boldsymbol{q}$ is $q_x = (2\pi/\lambda)(\cos\theta_i - \cos\theta_f)$ and its component normal to the surface, $q_z = (2\pi/\lambda)(\sin\theta_i + \sin\theta_f)$. For grazing incidence at a surface, however, the BA often fails. Nevertheless, the truncation effect of the surface plane allows us to write the scattered intensity in terms of the lateral projection q_x, $\boldsymbol{x}$ and the two projections, $p_i = (2\pi/\lambda)\sin\theta_i$ and $p_f = (2\pi/\lambda)\sin\theta_f$ of $\boldsymbol{k}_i$ and $\boldsymbol{k}_f$, respectively. The scattered intensities of neutron beams polarized parallel and anti-parallel to the applied field direction are different. Their contrast reveals the magnetism of the surface structure.

Layers laterally uniform within the in-plane projection of the coherence length give rise to specular reflection only, with $q_x = 0$, i.e. $\theta_i = \theta_f$. In this case, the scattering cross-section contains the δ-function $\delta(q_x)$, which provides the conservation of the neutron momentum along the ideally flat infinite surface. The proportionality coefficient at the δ-function is the reflectivity $R(q_z)$, which depends only on $q_z = (4\pi/\lambda)\sin\theta_i$.

For systems with chemical and/or magnetic structures that are not uniform across the surface, if the length scale of the variation is smaller than or comparable to the projection of the coherence length of the neutron beam along $\boldsymbol{x}$ (typically in the order of microns to tens of microns), significant off-specular scattering may occur. Such scattering has non-zero q_x component, and both specular and off-specular components must be analyzed to obtain the laterally resolved chemical/magnetic profile of the sample [4–6].

To illustrate the case of scattering from a surface with small length-scale lateral magnetic structures, we present here results of measurements on an array of rectangular permalloy ($Ni_{80}Fe_{20}$) bars patterned on a silicon substrate. An AFM image of the sample is shown in Fig. 1. The bars are 100 Å thick, 2 μm × 10 μm in lateral dimension and are separated by 2 μm. The coercive and saturation fields along the long axis (easy axis) of the bars are 12 and 30 Oe, respectively. This system is interesting as the magnetic domain size of permalloy is of the order of microns and therefore comparable to the element size. At saturation, on the other hand, it provides us with a simple magnetic system that produces many scattering features we are interested in. The measurements were performed with $H = 50$ Oe applied along the easy axis perpendicular to the scattering plane. Fig. 2 shows the scattered intensity as a function of neutron wavelength and scattering angle $2\theta = \theta_f + \theta_i$ for (a) spin-up and (b) spin-down incident beam. The measurements were carried out at a TOF polarized reflectometer, POSY 1 at the Intense Pulsed Neutron Source, Argonne National Laboratory. There was no polarization analysis of the reflected neutrons. The incident angle was $\theta_i = 1.08°$ and the specular reflection can be seen at $2\theta = 2\theta_i = 2.16°$. Two off-specular scattering fringes are evident: one at angles above the specular reflection ridge and the other between the specular ridge and

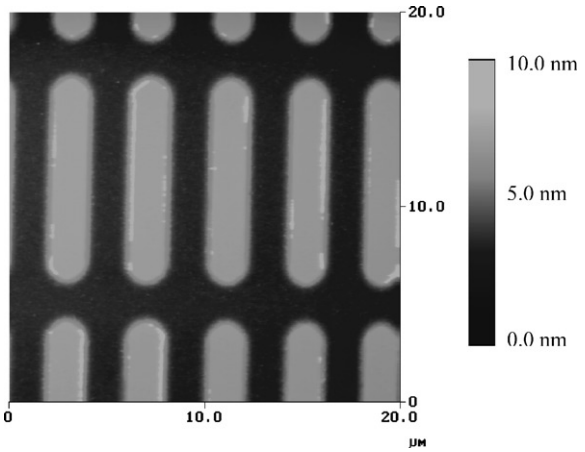

Fig. 1. AFM image of the micron-sized magnetic elements on a silicon surface.

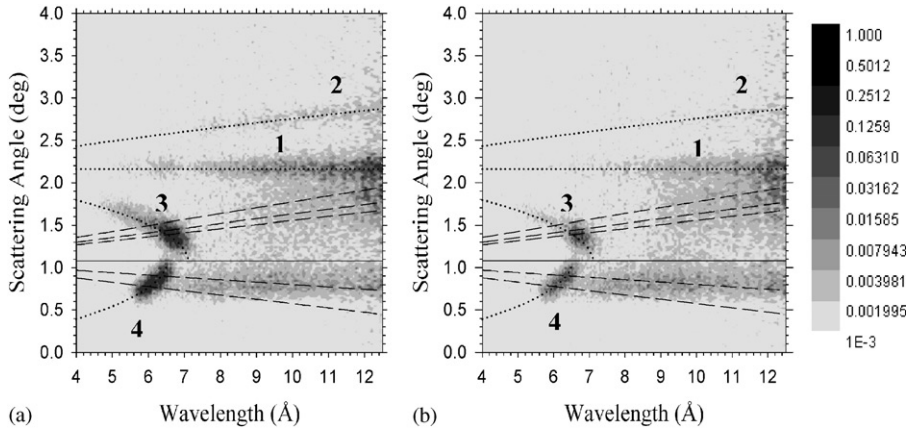

Fig. 2. Log-scale intensity map for (a) spin-up and (b) spin-down incident neutrons scattered from an array of micron-sized magnetic elements on a silicon surface. The solid line at 1.08° is the horizon. The dotted lines are calculated locations of: (1) specular reflection; (2, 3) off-specular reflections; and (4) diffraction. The dashed lines are the critical edges (from the horizon to higher/lower angles): the silicon edge (above the horizon only) and the permalloy edges corresponding to SLD Nb_{c+} and Nb_{c-}.

the 1.08° horizon. The fringes extend along lines given by

$$2\theta = \theta_i\sqrt{\theta_i^2 + 2n\lambda/d} \quad (1)$$

of the Bragg equation $q_x = 2\pi n/d$ for the two first-order ($n = \pm 1$) diffraction above the horizon. Diffraction patterns can also be seen below the horizon, where the first-order Bragg diffraction is positioned along the line given by

$$2\theta = \theta_i\sqrt{\theta_i^2 + 2n\lambda/d - \mathrm{Nb}\,\lambda^2/\pi}, \quad (2)$$

where $n = -1$, and $\mathrm{Nb} = 2.15 \times 10^{-6}\,\text{Å}^{-2}$ is the scattering length density (SLD) of silicon. Since the diffracted beam leaves the sample through the side edge of the substrate, the term $\mathrm{Nb}\,\lambda^2/\pi$ in Eq. (2) is needed in order to account for the refraction of the diffracted neutrons through the silicon substrate. In Fig. 2, the dotted lines passing through the off-specular scattering and the diffraction fringes were calculated using these equations with the d=4 μm period of the array.

The intensity distribution of the off-specular scattering can be described [4–6] in terms of the distorted-wave Born Approximation (DWBA), which properly takes into account optical effects totally ignored in Born Approximation. The importance of the optical effects is clearly seen in Fig. 2, where the diffraction effect is substantially enhanced in the vicinity of the total reflection edges. The distortions of incident waves are due to specular reflection from and refraction into the *mean* optical potential of the layers and the substrate averaged over their lateral structure. The deviations from the mean potential caused by lateral patterning, interfacial roughness, etc., are then considered as a perturbation, which scatters the refracted incident and reflected waves. In the vicinity of the total reflection edges, the refracted–reflected waves have amplitudes comparable with the refracted–incident waves and their constructive interference provides the Yoneda-type enhancement in the off-specular scattering including the Bragg diffraction from periodic lateral patterns.

The reflection critical edges, indicated in Fig. 2 by the dashed lines above the horizon, follow the equations below:

$$2\theta = \theta_i + \lambda/\lambda_{c\pm}, \quad (3)$$

where $\lambda_{c\pm} = \sqrt{\pi/\mathrm{Nb}_{c\pm}}$ are the critical neutron wavelengths of the total reflection *at normal incidence*, and $\mathrm{Nb}_{c\pm}$ are the SLD for the positive/negative spin projection onto the mean magnetization. For silicon, $\mathrm{Nb} = 2.15 \times 10^{-6}\,\text{Å}^{-2}$ and one finds $\lambda_c = 1.2 \times 10^3\,\text{Å}$. For saturated permalloy, $\mathrm{Nb}_{c+} = 11.5 \times 10^{-6}\,\text{Å}^{-2}$ and $\mathrm{Nb}_{c-} = 7.3 \times 10^{-6}\,\text{Å}^{-2}$. Taking into account the coverage fraction $c = 0.4$ of the permalloy bars over the surface, the mean optical potentials are

$\langle \mathrm{Nb}_{c_+^-} \rangle = 4.6 \times 10^{-6}\,\text{Å}^{-2}$ and $\langle \mathrm{Nb}_{c+} \rangle = 2.9 \times 10^{-6}\,\text{Å}^{-2}$, and correspondingly, $\lambda_{c+} = 0.8 \times 10^{3}$ Å and $\lambda_{c-} = 1.0 \times 10^{3}$ Å. From Fig. 2, one sees that the off-specular scattering intensities indeed receives appreciable enhancement near the intersections of the off-specular scattering ridge (dotted lines) and the reflection critical edges (dashed lines), while the intensity of the Bragg reflection above the specular ridge is not enhanced. Because the diffracted beam leaves the sample through the side edge of the substrate, the diffraction critical edges below the horizon, as determined by the optical contrast between the mean potentials of the permalloy and the substrate, are smaller than those above the horizon. These critical edges obey the equations

$$2\theta = \theta - \lambda/\lambda'_{c\pm}, \tag{4}$$

where the critical wavelength is now given by $\lambda'_{c\pm}\sqrt{\pi/(\mathrm{Nb}_{c\pm} - \mathrm{Nb})}$, with $\mathrm{Nb}_{c\pm}$ and Nb being the SLD for permalloy and silicon, respectively, as discussed above. The diffraction critical edges have a slope smaller then those above the horizon. Some scattering intensities along the critical edge lines, both above and below the horizon, are evident. The scattering originated from interfacial roughness or other lateral irregularities, and received an enhancement (Yoneda effect) in the vicinity of the total reflection. Above the horizon, the *Yoneda scattering* begins at $2\theta = \theta_i$ at $\lambda = 0$ and ends at $2\theta = 2\theta_i$ at $\lambda = \lambda_{c\pm}$, where the critical edge meets the specular ridge.

No higher orders of the Bragg diffraction were detected. One of the reasons is that the even-order reflections are suppressed: Starting from an edge of a permalloy bar, as we move along the x-direction on the surface, the deviation of the potential from its mean value changes sign every 2 μm while having the same amplitude. Even orders of the Bragg diffraction are forbidden if the spacing between the stripes equals the stripe width, as it is the case in our sample. For the same reason, the zero-order diffraction does not interfere with the reflection from the mean potential, which can easily be calculated exactly [4–6].

The measurement accuracy is not sufficient to detect any spin splitting of the critical edges due to birefringence. We cannot distinguish between λ_{c+} and λ_{c-}—neither above, nor below the horizon. However, the difference in the spin-up and spin-down intensities is a clear indication of the magnetic dependence of the SLD. More detailed comparison with theoretical calculations is currently underway.

In the above discussions, we focus on lateral magnetic structures that are small or comparable to the lateral coherence length of the neutron beam. Lateral magnetic structures, such as domains in a ferromagnetic thin film, can be large and there is little off-specular intensity. In this case, as detailed in a previous work [7], information on the lateral distribution of the magnetic domain orientations can still be obtained from the specular reflections. The normalized mean magnetization $\langle \cos\varphi \rangle$ and the domain dispersion, $\chi^2 = \langle \cos^2\varphi \rangle - \langle \cos^2\varphi \rangle^2$, where φ is a domain's magnetization angle measured from the applied field direction, is related to the reflectivities through the following relations:

$$\frac{R^{++} - R^{--}}{R_S^{++} - R_S^{--}} = \frac{R^{+} - R^{-}}{R_S^{+} - R_S^{-}} = <\cos\varphi>, \tag{5}$$

$$\frac{R^{-+}}{R_S^{-+}(90^\circ)} = <\sin^2\varphi>, \tag{6}$$

where the superscripts of the reflectivity R follow the usual convention for representing the polarization of the incident and reflected neutrons. The subscript S denotes values obtained at saturation, and $R_S^{-+}(90^\circ)$ is obtained when the magnetization of the saturated sample is turned perpendicular to the field $\boldsymbol{H}$ guiding the polarization. The dispersion provides a measurement of the width of the domain orientation distribution. The analysis was previously applied to an exchange-biased bilayer CoO(45 Å)/Co(130 Å) to study magnetization reversal processes at the reversal points [7]. The hysteresis loop is shown in the inset of Fig 3a. The interpretation of the data was simplified by having $\langle \cos\varphi \rangle = 0$ at the reversal points. In the current paper, the capability of the analysis is illustrated further in measurements made at locations other than the reversal. Reflectivities measured at locations before and after reversal, at +200 and +450 Oe, respectively, are presented in Fig. 3a and b. The magnetizations at the two fields are

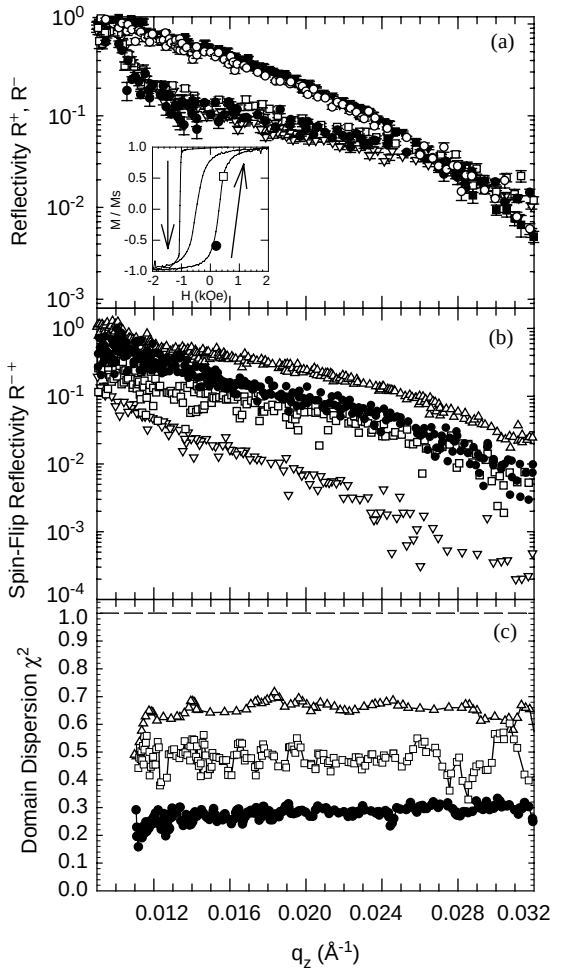

Fig. 3. Reflectivities of an exchange-biased CoO/Co bilayer at 10 K: (a) R^+ (filled symbols) and R^- (open symbols) at $H = +200$ Oe (circle), $+450$ Oe (square), and $+5$ kOe (lower triangle); (b) R^{-+} at $H = +200$ Oe (filled circle), $+450$ Oe (square), $+5$ kOe (lower triangle), and $R^{-+}(90°)$ (upper triangle). The inset in (a) shows the hysteresis (solid line) at 10 K and the normalized magnetization obtained from R^+ and R^-. (c) Magnetic domain dispersion χ^2 of the CoO/Co bilayer at 10 K and $H = +200$ Oe (filled circle), and $+450$ Oe (square). Data taken at reversal at $+350$ Oe is included for comparison (upper triangle).

plotted in the inset of Fig. 3a. These values were obtained by applying Eq. (5) to the data and they are in agreement with measurements obtained using a standard magnetometer. The domain dispersions at the two fields are shown in Fig. 3c (data at the reversal are also plotted for comparison). While it may be intuitive to expect the dispersion to increase as the applied field increases towards the coercive field, and to decrease after passing the reversal point, quantitative measurements allow us to make concise comparison with theory such as the Stoner–Wohlfarth theory of magnetic domains [8]. Currently, there are few techniques beside PNR that allow us to obtain the lateral domain dispersion.

In conclusion, we have shown how PNR-TOF can be applied to study lateral magnetic structures on a surface. For structures with small length scales, we evaluate the off-specular scattering from array of micron-sized magnetic elements. For large length-scale structures, we illustrate how to obtain the ferromagnetic domain dispersion of an exchange biasing CoO/Co bilayer film along the hysteresis loop.

Acknowledgements

Work done at Argonne National Laboratory was supported by US DOE, Office of Science contract #W-31-109-ENG-38 and by Oak Ridge National Laboratory, managed for the US D.O.E. by UT-Battelle, LLC under Contract No. DE-AC05-00OR22725. W.-T. Lee and F. Klose would like to acknowledge the contributions of S.G.E. te Velthus, G.P. Felcher, T. Gredig, and E.D. Dahlberg in works related to the Co/CoO.

References

[1] J.F. Ankner, G.P. Felcher, J. Magn. Magn. Mater 200 (1999) 741.
[2] C.F. Majkrzak, Physica B 221 (1996) 342.
[3] H. Zabel, R. Siebrecht, A. Schreyer, Physica B 276 (2000) 17.
[4] B.P. Toperverg, Physica B 297 (2001) 160.
[5] B.P. Toperverg, G.P. Felcher, V.V. Metlushko, V. Leiner, R. Siebrecht, O. Nikonov, Physica B 283 (2000) 149.
[6] B.P. Toperverg, Polarized Neutron Reflection and Off-Specular Scattering in Polarized Neutron Scattering, Forschungszentrum Jülich, Series "Matter and Materials", Vol. 12, 2002.
[7] W.-T. Lee, S.G.E. te Velthuis, G.P. Felcher, F. Klose, T. Gredig, D. Dahlberg, Phys. Rev. B 65(22) (2002); art. no. 224417.
[8] E.C. Stoner, E.P. Wohlfarth, Philos. Trans. R. Soc. London Ser. A 240 (1948) 599.